Eastward and Westward Flows Over Topography in Nonlinear and Linear Barotropic Models

J. S. FREDERIKSEN

CSIRO, Division of Atmospheric Physics, Aspendale, Victoria, Australia

(Manuscript received 9 March 1982; in final form 22 June 1982)

ABSTRACT

The transient and stationary flow fields produced when initial zonal solid body rotation currents flow over topography is studied in spherical barotropic models for eastward and westward flow directions and with variable and constant Coriolis parameters (f). Fully nonlinear analytical solutions are obtained using the methods of equilibrium statistical mechanics and are compared with linearized solutions and with the qualitative results of previous laboratory and numerical experiments.

The equilibrium solutions show that westward flow with variable f is stable in the sense that only very small amplitude transients are produced and the initial flow is practically unchanged. The stationary streamfunction dominates the total flow field and there is excellent agreement with linear steady state solutions and with the qualitative results of laboratory and numerical experiments.

For eastward flow with variable f, the equilibrium solutions demonstrate that the flow is unstable; that is, large amplitude transients are produced and the zonal flow direction changes to westward. The transients dominate the total eddy flow field while the smaller amplitude stationary eddy streamfunction is essentially a filtered version of the topography and is very similar to that for initial westward flow. In contrast, the linear steady state solutions are resonant or near resonant and differ dramatically from the nonlinear stationary solutions. The meaning of the linear steady state solutions is discussed and comparisons are made of linear transient and nonlinear equilibrium solutions with laboratory and numerical experiments.

With constant f, the equilibrium solutions show that eastward flow again reverses to westward while westward flow remains that way but decreases its strength. The amplitudes of the transients for the two flow directions are now comparable and are considerably less than for the case of eastward flow with variable f. For both flow directions the transient and stationary eddy energy spectra are strongly peaked at zonal wavenumber $|m| = 1$ with the stationary spectrum being dominant. The corresponding linear steady state solutions have a resonance at $|m| = 1$ when the flow is inviscid and large amplitude there when viscosity is included.

1. Introduction

During the early 1950's, a number of laboratory experiments were conducted by Fultz and Long (1951), Long (1952), Fultz and Frenzen (1955) and Frenzen (1955) with the view of understanding the influence of mountain barriers upon atmospheric flow patterns. In their experiments, they studied the essentially two-dimensional motions of a homogeneous fluid past obstacles in a rotating hemispherical shell. Among their more striking findings was the fact that when the zonal current flows eastward over the obstacle, trains of waves are produced downstream of the obstacle while westward flow is little disturbed by the obstacle. Subsequently, a number of numerical experiments using barotropic models have been carried out by Kasahara (1966), Egger (1970), Vergeiner and Ogura (1972) and Edelmann (1972) with the specific view of further elucidating the different transient behaviors produced by eastward and westward flows over obstacles.

The qualitatively different transient behaviors produced by eastward and westward zonal flows over obstacles may be understood in a general way using potential vorticity conservation arguments (Kasahara, 1966; Holton, 1979); comparisons between numerical experiments and linear steady state theory have also been carried out (e.g., Kasahara, 1966). However, it appears that there have been no studies of this phenomenon using semi-analytical methods capable of dealing with the fully nonlinear equations. It was shown in Frederiksen and Sawford (1980, 1981, hereafter FS1 and FS2, respectively) that the methods of equilibrium statistical mechanics may be used to obtain analytic solutions for the expected asymptotic behavior of flow described by the inviscid spherical barotropic model in the presence or absence of topographic forcing. It is the purpose of this article to use these methods to study eastward and westward flows over topography in the barotropic model and to compare the statistical mechanical equilibrium solutions with linear steady state solutions and with previous numerical experiments.

The linear steady state solutions are studied in both

0022-4928/82/112477-13$07.25

the presence and absence of viscous dissipation; however, it should be emphasized that the nonlinear equilibrium solutions neglect the effect of viscosity, which is undoubtedly important for atmospheric flows. The statistical behavior of flows in the presence of viscosity can also be formulated by using various closure approximations such as the direct interaction approximation or the eddy-damped quasi-normal Markovian approximation (Kraichnan, 1959; Leith 1971; Leslie 1973; Carnevale and Frederiksen, 1982 and references therein). However, the formulation and in particular the solution of these statistical closure equations is quite complicated when the flow is inhomogeneous and anisotropic. The other main reason for restricting our attention to inviscid equilibrium solutions is that they can be derived rigorously and are not dependent on closure assumptions. Furthermore, it was found in FS1 and FS2 that, with a resolution defined by a rhomboidal truncation wavenumber $J = 15$, the observed and equilibrium spectra were in reasonable agreement for a range of intermediate wavenumbers.

The plan of the paper is as follows. In Section 2 we summarize the nonlinear equilibrium and linear steady state solutions to the barotropic model in the presence of topographic forcing and for initial solid body rotation flows. The energy spectra of the statistical mechanical equilibrium solutions are studied in Section 3 for both variable and constant Coriolis parameters (f). In Sections 4 and 5 the stationary and transient eddy streamfunctions for the nonlinear equilibrium solutions are compared with the linear solutions and with the qualitative results of previous laboratory and numerical simulation experiments. Results for variable f are presented in Section 4 and for constant f in Section 5. The conclusions are summarized in Section 6.

2. Theory

a. Model details

The nondimensional equations defining the spherical equivalent barotropic model are

$$\frac{\partial \nabla^2 \psi}{\partial t} + J(\psi, \nabla^2 \psi + 2\mu + h) = 0, \tag{2.1a}$$

where

$$h = 2\mu g A H / R T_0 , \tag{2.1b}$$

$$J(f, g) = \frac{\partial f}{\partial \lambda}\frac{\partial g}{\partial \mu} - \frac{\partial f}{\partial \mu}\frac{\partial g}{\partial \lambda}. \tag{2.1c}$$

Here we have taken a_0 (earth's radius) and Ω^{-1} (earth's angular velocity)$^{-1}$ as length and time scales. In (2.1), ψ is the streamfunction, $\mu = \sin(\text{latitude})$, λ is the longitude, t the time, H the height of the topography, R the gas constant for air, T_0 the horizontally-averaged surface temperature, g the acceleration due to gravity and A the value of the vertical profile factor at 1000 mb. As in FS2, we can use the following values of the various parameters:

$$\left.\begin{aligned} A &= 0.8 \\ R &= 287 \text{ J kg}^{-1} \text{ K}^{-1} \\ T_0 &= 273 \text{ K} \end{aligned}\right\}. \tag{2.1d}$$

Eq. (2.1) may be written in spectral form by expanding both the streamfunction and the forcing function $\hat{h} = 2\mu + h$ in spherical harmonics:

$$\psi = \sum_{m=-J}^{J} \sum_{n=|m|}^{|m|+J} \psi_{mn} P_n^m(\mu) e^{im\lambda}, \tag{2.2a}$$

$$\hat{h} = 2\mu + h = \sum_{m=-J}^{J} \sum_{n=|m|}^{|m|+J} \hat{h}_{mn} P_n^m(\mu) e^{im\lambda}. \tag{2.2b}$$

This gives

$$\left.\begin{aligned} -n(n+1)\frac{\partial \psi_{mn}(t)}{\partial t} &= i \sum_p \sum_q \sum_r \sum_s K_{nqs}^{mpr} \psi_{rs}(t) \hat{h}_{pq} \\ &+ \frac{i}{2} \sum_p \sum_q \sum_r \sum_s [s(s+1) - q(q+1)] \\ &\times K_{nqs}^{mpr} \psi_{rs}(t) \psi_{pq}(t) \end{aligned}\right\}. \tag{2.3}$$

In these equations, $\psi_{-mn} = \psi_{mn}^*$ and $\hat{h}_{-mn} = \hat{h}_{mn}^*$ since we take $P_n^{-m}(\mu) = P_n^m(\mu)$ where $P_n^m(\mu)$ are orthonormalized Legendre functions and ψ_{mn} and $\hat{h}_{mn}$ are spectral amplitudes, m is the zonal wavenumber, n the total wavenumber and J is the rhomboidal truncation wavenumber. Since it was found in FS1 and FS2 that the observed atmospheric and equilibrium spectra were in reasonable agreement for a range of intermediate wavenumbers when $J = 15$ was used, we shall also employ that truncation throughout this article. The interaction coefficient K_{nqs}^{mpr} is defined in Eq. (2.3) of FS1.

b. Equilibrium solutions

Details of the derivation of the equilibrium solutions are given in FS1 and FS2. The essential requirements are that the probability distribution function satisfies Liouville's equation [Eq. (3.6) of FS1], which may be established from Eq. (2.3), and the fact that the truncated equations conserve kinetic energy

$$\mathcal{E} = \tfrac{1}{4} \sum_{m=-J}^{J} \sum_{n=|m|}^{|m|+J} n(n+1) \psi_{mn} \psi_{mn}^* \tag{2.4a}$$

and potential enstrophy

$$\mathcal{F} = \tfrac{1}{4} \sum_{m=-J}^{J} \sum_{n=|m|}^{|m|+J} |-n(n+1)\psi_{mn} + \hat{h}_{mn}|^2. \tag{2.4b}$$

The invariants of Eqs. (2.1) and (2.3) may be established using the method of Thompson (1974), generalized to spherical geometry and to include topog-

raphy, and the method described in the appendix of Sawford and Frederiksen (1982).

The equilibrium solutions are ensemble averages over a large number of realizations of the system with the same $\mathcal{E}$ and $\mathcal{T}$ and which are equivalent to long-time averages over a single realization (FS1; Sawford and Frederiksen, 1982 and references therein). The expectation values of the spectral coefficients are given by

$$\langle \psi_{mn} \rangle = \frac{\beta \hat{h}_{mn}}{\alpha + \beta n(n+1)} \tag{2.5}$$

while the expectations of the kinetic energy and potential enstrophy of the (m, n) and $(-m, n)$ modes are

$$E_{mn} = E_{-mn} = \frac{1}{2[\alpha + \beta n(n+1)]} + \frac{1}{4} n(n+1) |\langle \psi_{mn} \rangle|^2, \tag{2.6a}$$

$$F_{mn} = F_{-mn} = \frac{1}{2} \frac{n(n+1)}{\alpha + \beta n(n+1)} + \frac{1}{4} \frac{\alpha^2}{\beta^2} |\langle \psi_{mn} \rangle|^2. \tag{2.6b}$$

The parameters α, β are determined by equating the expectations for the total energy and potential enstrophy to the invariant values $\mathcal{E}$ and $\mathcal{T}$ determined by the initial conditions. The positivity of the probability distribution also requires that $\alpha + \beta n(n+1)$ is positive. We note that similar equilibrium solutions exist in planar geometry (Salmon *et al.*, 1976).

As discussed in FS2, the expectation of the transient part of the streamfunction field is zero while Eq. (2.5) gives the stationary part. Also, the second terms on the right-hand sides of Eqs. (2.6a) and (2.6b) represent contributions to the energy and potential enstrophy from the stationary part of the flow, while the first terms represent the transient contributions.

As in FS2, since our resolution is not too coarse, β is positive and the streamfunction field is positively correlated with the forcing field $\hat{h}$ at all scales. It is, in fact, a filtered version of the forcing field in the sense that the streamfunction coefficients are simply positive multiples of the forcing field coefficients with the scaling depending on n.

In the following sections we shall also consider the case where the Coriolis parameter ($f = 2\Omega\mu$) in Eq. (2.1a) does not vary with latitude, i.e. $2\mu \to 2\mu_0$ where μ_0 is a constant. This of course leads to a drastic change in $\hat{h}_{01}$ as seen from Eq. (2.2b) since $|h_{01}| \ll 2\sqrt{2/3}$. We shall see in the following sections that this change is reflected in the nature of the equilibrium solutions.

We note that there is no numerical evidence that any other statistical mechanical equilibrium solution (which survives under the addition of small random perturbations to the initial conditions) exists for Eq. (2.3) (cf. FS2; Egger and Metz, 1981; Sawford and Frederiksen, 1982 and references therein). In fact, Carnevale (1979) and Carnevale *et al.* (1981) have proved a Boltzmann-type H-theorem for inviscid barotropic flow over topography described by the eddy-damped quasi-normal Markovian equation which is a statistical closure derived from the basic field equations. This theorem states that the entropy of the flow will increase until the statistical mechanical equilibrium solution is reached.

c. *Linear solution in presence of drag and diffusion*

In the following sections we shall analyze the linear solutions of Eq. (2.1) both for the inviscid case given there and also in the presence of drag and diffusion. With these terms present, the linear barotropic equation becomes

$$\frac{\partial \nabla^2 \psi'}{\partial t} + J(\bar{\psi}, \nabla^2 \psi' + \hat{h}) + J(\psi', \nabla^2 \bar{\psi} + 2\mu) + \kappa \nabla^2 \psi' + \kappa' \nabla^6 \psi' = 0. \tag{2.7a}$$

Here $\bar{\psi}$ is the basic state streamfunction which specifies the zonal flow and we let

$$\psi' = \psi^S + \psi^T, \tag{2.7b}$$

where ψ^S is a stationary eddy field whose time tendency vanishes and ψ^T is a transient eddy field which satisfies the homogeneous equation corresponding to (2.7) (i.e., with the replacement $\hat{h} \to 0$). In this paper we shall restrict our attention to the special case when the zonal flow is solid body rotation

$$\bar{\psi} = \bar{\psi}_{01} P_1^0(\mu) = -\gamma\mu, \tag{2.8a}$$

where

$$\gamma = -\sqrt{3/2}\,\bar{\psi}_{01}. \tag{2.8b}$$

As in FS2, we use the nondimensional drag and diffusion coefficients

$$\kappa = 0.011507, \quad \kappa' = 1.946 \times 10^{-7} \tag{2.9}$$

throughout. Then with the expansions

$$\psi^S = \sum_{m>0} \sum_n \psi^S_{mn} P_n^m(\mu) e^{im\lambda}, \tag{2.10a}$$

$$\psi^T = \sum_{m>0} \sum_n \psi^T_{mn} P_n^m(\mu) e^{i[m\lambda - \omega(m,n)t]}, \tag{2.10b}$$

$$\hat{h} = \sum_{m>0} \sum_n \hat{h}_{mn} P_n^m(\mu) e^{im\lambda}, \tag{2.10c}$$

we find that the stationary spectral components satisfy the equation

$$\psi^S_{mn} = \gamma \hat{h}_{mn} \{\gamma n(n+1) - 2(\gamma + 1) - i[\kappa n(n+1) + \kappa' n^3 (n+1)^3]/m\}^{-1}, \quad m > 0. \tag{2.11}$$

In order for the transient solution to satisfy the ho-

TABLE 1. Values of the initial zonal wind at the equator, u_i (m s^{-1}) and the corresponding nondimensional $\bar{\psi}_{01}$ and γ for solid body rotation. Also shown for eastward flow is the resonant total wavenumber n_r defined by $n_r(n_r + 1) = 2(\gamma + 1)/\gamma$.

u_i	±27.5	±15.0	±7.8
$\bar{\psi}_{01}$	∓0.048385	∓0.02645	∓0.013752
γ	±0.959259	±0.032389	±0.016842
n_r	5.5	7.5	10.5

mogeneous equation, the angular frequency must satisfy the equations

$$\omega(m, n) = \omega_r + i\omega_i, \tag{2.12a}$$

where

$$\omega_r = mc_r = m\gamma - \frac{2m(\gamma + 1)}{n(n + 1)}, \quad m > 0, \tag{2.12b}$$

$$\omega_i = -\kappa - \kappa' n^2(n + 1)^2, \tag{2.12c}$$

We also note that if one considers the linear initial value problem where at time $t = 0$ the flow is pure solid body rotation with no eddies present, then one has

$$\psi^T_{mn} = -\psi^S_{mn}, \quad m > 0. \tag{2.13}$$

d. Comparison of linear and nonlinear stationary solutions

In the absence of drag and diffusion, Eq. (2.11) reduces to

$$\psi^S_{mn} = \gamma\hat{h}_{mn}[-2(\gamma + 1) + \gamma n(n + 1)]^{-1}, \quad m > 0. \tag{2.14}$$

Thus for *eastward* flow where $\gamma > 0$, we see that the linear solution has the same form as the nonlinear solution (2.5) with the replacements $\gamma \to \beta$, $-2(\gamma + 1) \to \alpha$. However, as discussed in FS2, while Eq. (2.5) implies a positive correlation at all scales between the topography and the streamfunction amplitudes since $\alpha + \beta n(n + 1) > 0$, for the linear case long waves with $-2(\gamma + 1) + \gamma n(n + 1) < 0$ are negatively correlated with the topography. In fact, the linear solutions have a resonance or near resonance for n near n_r where $n_r(n_r + 1) = 2(\gamma + 1)/\gamma$. Thus, for *eastward* flow, the effect of topographic forcing on scales with total wavenumber near n_r and zonal wavenumber up to $m \approx n_r$ is enhanced in the linear solutions.

For *westward* flow where $\gamma = -\Gamma$ with $\Gamma > 0$, Eq. (2.14) becomes

$$\psi^S_{mn} = \Gamma\hat{h}_{mn}[2(1 - \Gamma) + \Gamma n(n + 1)]^{-1}, \quad m > 0 \tag{2.15}$$

and the linear and nonlinear solutions have the same form with $2(1 - \Gamma)/\Gamma \to \alpha/\beta$. Also, since $2(1 - \Gamma) + \Gamma n(n + 1) > 0$, there is a positive correlation at all scales between the topography and the streamfunction amplitudes just as there is for the statistical mechanical solution (2.5). Thus for *westward* solid body rotation flow, the main differences between the stationary statistical mechanical equilibrium eddy solutions and the linear inviscid eddy solutions arise through any differences in $2(1 - \Gamma)/\Gamma$ compared with α/β.

e. Linear solution with constant Coriolis parameter

When the Coriolis parameter in Eq. (2.7) does not vary with latitude, i.e. $2\mu \to 2\mu_0$ where μ_0 is constant, then the analysis of Section 2c again applies with $(\gamma + 1)$ replaced by γ in Eqs. (2.11) and (2.12b). In particular, the inviscid stationary solution for both eastward and westward flow is given by

$$\psi^S_{mn} = \hat{h}_{mn}[n(n + 1) - 2]^{-1}, \quad m > 0, \tag{2.16}$$

which diverges at $n = 1$ giving resonant modes ψ_{11} and ψ_{-11}. When relatively weak drag and diffusion are present, this in general means that ψ_{11} and ψ_{-11} will have large moduli.

3. Energy spectra of statistical mechanical equilibrium solutions

For all the flow configurations studied in this article we suppose that the initial flows consist of purely solid body rotation with no eddies present. Then both the linear and nonlinear statistical solutions are uniquely determined by the initial zonal flow and topography, as may be seen from Eqs. (2.11) and (2.4)–(2.6). The initial solid body rotation profiles that we shall employ are specified by

$$u(\phi, t = 0) = u_i \cos\phi, \tag{3.1}$$

where ϕ is latitude and u_i is the dimensional zonal wind at the equator. The calculations will be for global flow throughout. Table 1 shows the values of u_i used and the corresponding $\bar{\psi}_{01}$, γ and n_r. Throughout we use the same topography as in Section 4 of FS2, i.e., a circular conical mountain taken to be 2500 m high, centered at 30°N, 180°W with a diameter of 45° latitude (it is depicted by the dashed lines in Fig. 4). The statistical mechanical equilibrium solutions are uniquely determined by α and β which in turn require for their calculation the total energy $\mathcal{E}$ and potential enstrophy $\mathcal{T}$. These are calculated from Eq. (2.4) with only $\psi_{01} = \bar{\psi}_{01}$ nonzero. Table 2 gives the values of $\mathcal{E}$ and $\mathcal{T}$ and the corresponding α, β and α/β for each of the initial zonal flow cases in Table 1. Also shown are the dimensional equilibrium expectation values $\langle u_{01}\rangle$ given by

$$\langle u_{01}\rangle = -\sqrt{3/2}\langle\psi_{01}\rangle a_0\Omega, \tag{3.2}$$

where $\langle\psi_{01}\rangle$ is given in Eq. (2.5). The quantities in Table 2 which refer to the constant Coriolis parameter case have been given a subscript 0.

TABLE 2. Values of the dimensional total energy ($\mathcal{E}a_0^2\Omega^2$) in $m^2\ s^{-2}$, potential enstrophy ($\mathcal{T}\Omega^2$) in s^{-2} and the nondimensional parameters α, β and the ratio α/β for different initial zonal winds u_i. Also shown are the equilibrium expectation values of the zonal wind at the equator $\langle u_{01}\rangle$ in m s^{-1}. The quantities with superscript zero refer to solutions for constant f.

u_i (m s^{-1})	+27.5	−27.5	+15.0	−15.0	+7.8	−7.8
$\mathcal{E}a_0^2\Omega^2$ } $\mathcal{E}^0a_0^2\Omega^2$ }	252.7	252.7	75.5	75.5	20.4	20.4
$\mathcal{T}\Omega^2$ (s^{-2})	4.002×10^{-9}	3.160×10^{-9}	3.803×10^{-9}	3.342×10^{-9}	3.689×10^{-9}	3.450×10^{-9}
α	8.070×10^{4}	7.444×10^{7}	3.647×10^{5}	1.979×10^{8}	2.194×10^{6}	6.050×10^{8}
β	1.457×10^{3}	2.334×10^{6}	2.289×10^{3}	3.297×10^{6}	1.688×10^{3}	5.153×10^{6}
α/β	5.539×10^{1}	3.189×10^{1}	1.593×10^{2}	6.002×10^{1}	1.300×10^{3}	1.174×10^{2}
$\langle u_{01}\rangle$	−16.2	−27.5	−5.78	−15.0	−0.716	−7.8
$\mathcal{T}^0\Omega^2$ (s^{-2})	1.518×10^{-11}	1.253×10^{-11}	5.844×10^{-12}	4.399×10^{-12}	2.784×10^{-12}	2.032×10^{-12}
α^0	-4.437×10^{5}	-8.859×10^{5}	-5.969×10^{5}	-1.013×10^{6}	-6.015×10^{5}	-8.874×10^{5}
β^0	2.479×10^{5}	4.944×10^{5}	3.722×10^{5}	6.301×10^{5}	5.304×10^{5}	7.615×10^{5}
α^0/β^0	−1.790	−1.792	−1.604	−1.608	−1.151	−1.165
$\langle u^0_{01}\rangle$	−13.9	−14.1	−7.39	−7.45	−3.45	−3.51

Given $\mathcal{E}$, $\mathcal{T}$ and the topographic field, the qualitative nature of the solutions may be understood analytically as described in Sawford and Frederiksen (1982). Figs. 1a, b and c show the transient, stationary and total kinetic energy spectra as a function of zonal wavenumber for initial solid body rotation flows with $|u_i| = 15.0$ m s^{-1} while Figs. 2 and 3 show the total kinetic energy spectra for $|u_i| = 27.5$ and $|u_i| = 7.8$ m s^{-1}, respectively. From Fig. 1a it is evident that for eastward initial flow with variable Coriolis parameter f, a much larger proportion of the initial energy is distributed among transient eddies than for the other three cases considered. Of these, least eddy transient energy occurs for westward initial flow with variable Coriolis parameter. For the two cases with constant f, the equilibrium values of the transient kinetic energy are quite similar and have magnitudes which lie between those for initial eastward and westward flow with variable f. However, even with constant f the initial eastward flow yields larger transient energy at equilibrium.

In contrast, for initial eastward flow with variable f, the stationary component of the equilibrium energy is the smallest of the four cases. Again the two cases with constant f have very similar stationary energies at equilibrium. For the initial westward flow with variable f a large proportion of the stationary energy at equilibrium is contributed by the zonal flow which is dominated by the u_{01} component. Note that the slight differences in both the transient and stationary spectra between the two cases with constant f are due to small differences in the potential enstrophy produced by the small but nonzero h_{01} component.

From Fig. 1 we see that the total energy is dominated by the transient kinetic energy for all cases $m > 0$ when the initial flow is eastward with variable f. The zonal kinetic energy is again dominated by the stationary component due to the large $\hat{h}_{01}$ component produced by the variable f. For the other three cases the short-wave total kinetic energies are again dominated by the transient energies, while for the zonal flow and the larger scales the stationary kinetic energy dominates in the total energy. The large scale stationary kinetic energy makes the largest contribution to the total energy. These same observations apply to the corresponding cases shown in Figs. 2 and 3 for which $|u_i| = 27.5$ m s^{-1} and $|u_i| = 7.8$ m s^{-1} respectively. In particular, for the cases of eastward initial flow with variable f, the total transient kinetic energies are practically the same for $m > 0$. Thus, comparing Figs. 1a or c with Figs. 2 and 3, we see that as the initial zonal velocity u_i increases, the transient and total kinetic energy spectra become steeper (for $m > 0$) and the contribution of the larger eddies becomes relatively more important. The transient energy spectra correspond in each case to an (approximate) equipartition of potential enstrophy.

We may also consider the change in u_{01} and the generation of transients as *nonlinear* instability. If we define a measure of the nonlinear instability of the initial flow as $u_i - \langle u_{01}\rangle$, we see from Table 2 that eastward flows with variable f are most unstable while westward flows with variable f are practically stable. Eastward flows with constant f rank second in instability while westward flows rank third. It is clear that the instability is topographic in nature since, in the absence of topography, the component ψ_{01} is conserved (FS1) and the flow is stable for both eastward and westward solid body rotation.

It is evident from the spectra in Figs. 1–3 and from Table 2 that the statistical mechanical equilibrium solutions are consistent with practically all of the qualitative findings of the laboratory and numerical experiments mentioned in the Introduction, despite the fact that in some of these experiments viscosity plays some role and the geometry is different. Moreover, the integration in some of the numerical experiments, e.g., that of Kasahara (1966) which we shall discuss in some detail, was not carried out for long enough for the largest scales to reach equilibrium. Edelmann (1972) integrated his barotropic equations for considerably longer time. In particular, in Section 13 he describes an experiment in which

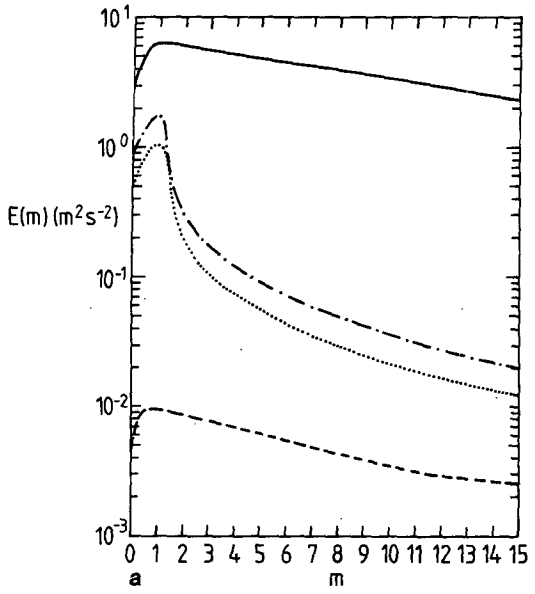

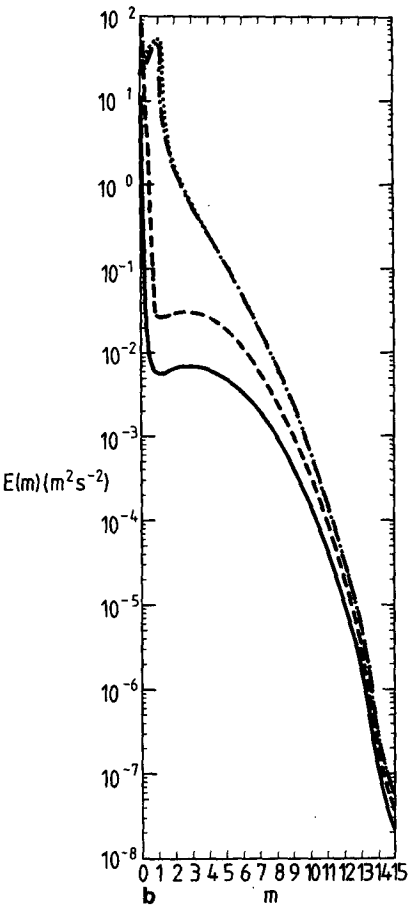

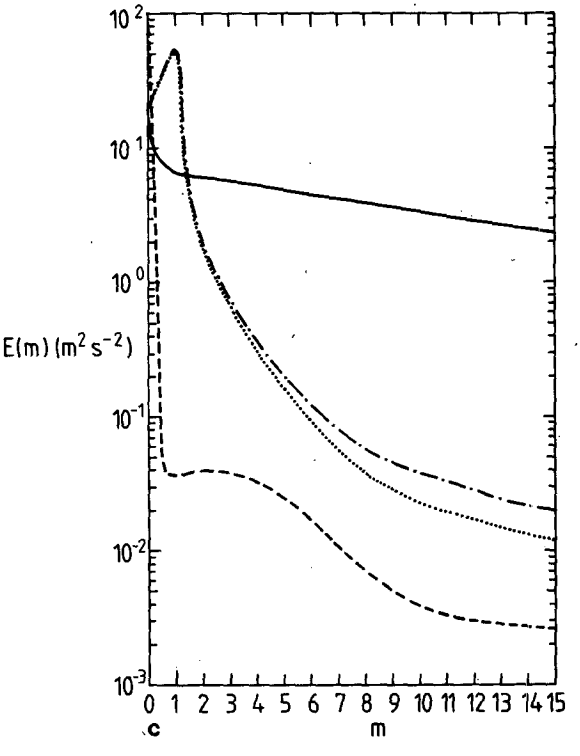

FIG. 1. Equilibrium kinetic energy spectra as a function of zonal wavenumber for (a) transient energy, (b) stationary energy and (c) total energy and with initial zonal wind $|u_i| = 15.0$ m s^{-1}. The solid and dashed lines refer respectively to eastward and westward initial flows with variable f, and the dot-dashed and dotted lines refer to eastward and westward initial flows with constant f.

an initial eastward flow is integrated, until after two months it has reversed direction to a westward large scale flow with transients.

We may summarize the findings in Figs. 1–3 and Table 2 as follows:

(1) Eastward flow with variable f over the topography produces large amplitude transients and the flow direction eventually reverses to westward.

(2) The relative importance of the various scales of the transients produced with initial eastward flow with variable f depends on the strength of the initial flow. The stronger the initial flow the greater is the dominance of long transient waves.

(3) Westward flow with variable f over topography produces few transients and the initial flow is practically unchanged.

(4) With constant f, both initial eastward and westward flows produce considerably less transients than occur with initial eastward flow and variable f. Also, the transients that are produced have spectra that are strongly peaked at zonal wavenumber $m = 1$.

In order to make a more direct comparison between the statistical mechanical equilibrium solutions and the qualitative results of Kasahara (1966) and Edelmann (1972), we consider in the next two sections the eddy streamfunctions corresponding to the results in Figs. 1–3. We also compare them with the linear solutions.

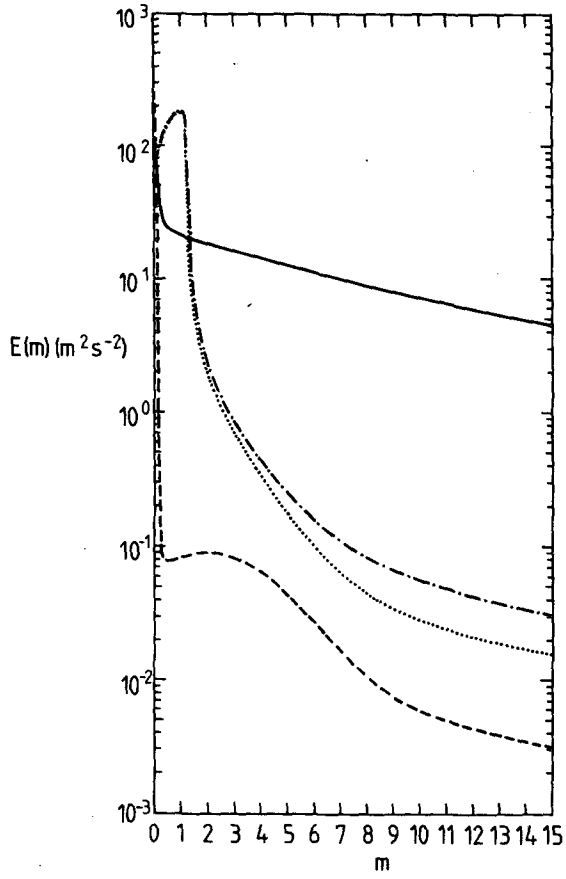

FIG. 2. As in Fig. 1, but for total kinetic energy when $|u_i| = 27.5$ m s^{-1}.

4. Nonlinear and linear solutions with variable Coriolis parameter

In this section we study the statistical mechanical equilibrium streamfunctions for variable Coriolis parameter and compare them with the linear solutions.

a. Nonlinear equilibrium solutions

Figs. 4a and b show the transient random phase eddy ($m \neq 0$) streamfunctions for eastward and westward flows with $|u_i| = 15.0$ m s^{-1}. The moduli of the transient eddy streamfunction coefficients ψ_{mn} are obtained from the transient energy [first term on the right-hand side of Eq. (2.6a)] and the phases are taken as random. The same random number seed has been used for both cases. It is clear that for eastward flow the transient eddy field is nearly 30 times stronger than for westward flow. For the other flow cases in Table 1, a similar situation exists. In addition, the result found by Kasahara (1966) that the longer transient waves become more important as the intensity of the initial eastward flow increases, and vice versa, is also borne out by the other transient eddy fields (not shown). It should be noted that in Kasahara's integrations the larger scales have not had time to approach equilibrium.

Fig. 5 shows the stationary eddy streamfunction for westward flow with $|u_i| = 15.0$ m s^{-1}; for eastward initial flow it is very similar qualitatively but with a reduced maximum value of 325×10^4 m^2 s^{-1}. In both cases the eddy streamfunction is a filtered version of the topography [cf. Eq. (2.5)].

b. Linear solutions

Fig. 6 shows the linear steady state eddy streamfunction for eastward initial flow with $u_i = 15.0$ m s^{-1}. (corresponding to a resonant total wavenumber $n_r = 7.5$) with drag and diffusion present. Without drag and diffusion present, the corresponding eddy geopotential was shown in Fig. 8 of FS2. The quasi-resonant behavior discussed in FS2 occurs, with drag and diffusion having quite a dramatic effect on the solution. For the other cases of eastward initial flow with $u_i = 27.5$ m s^{-1} ($n_r = 5.5$) and $u_i = 7.8$ m s^{-1} ($n_r = 10.5$), the linear steady state solutions are qualitatively similar to that in Fig. 6 (and Fig. 8 of FS2), but with the larger ($n_r = 5.5$) or smaller ($n_r = 10.5$) scales more important.

Fig. 7 shows the linear steady state solutions for westward initial flow with $u_i = -15.0$ m s^{-1} and with drag and diffusion included. Without drag and diffusion there is little difference from the above except that the maximum value is 667×10^4 m^2 s^{-1}. We see

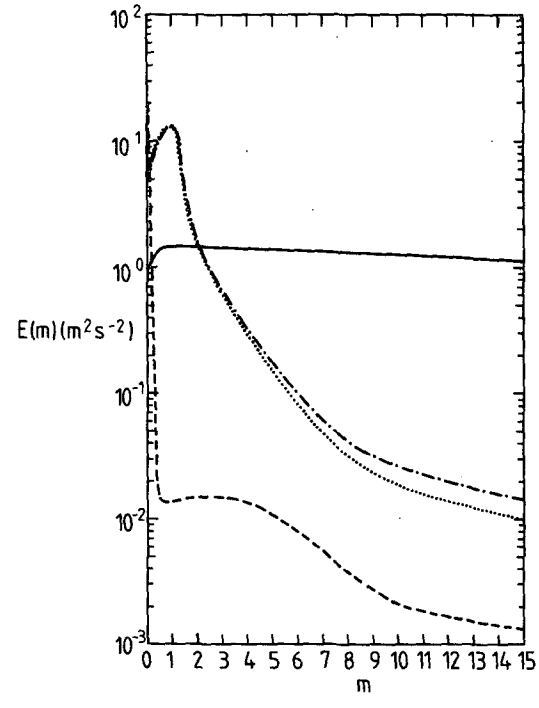

FIG. 3. As in Fig. 1, but for total kinetic energy when $|u_i| = 7.8$ m s^{-1}.

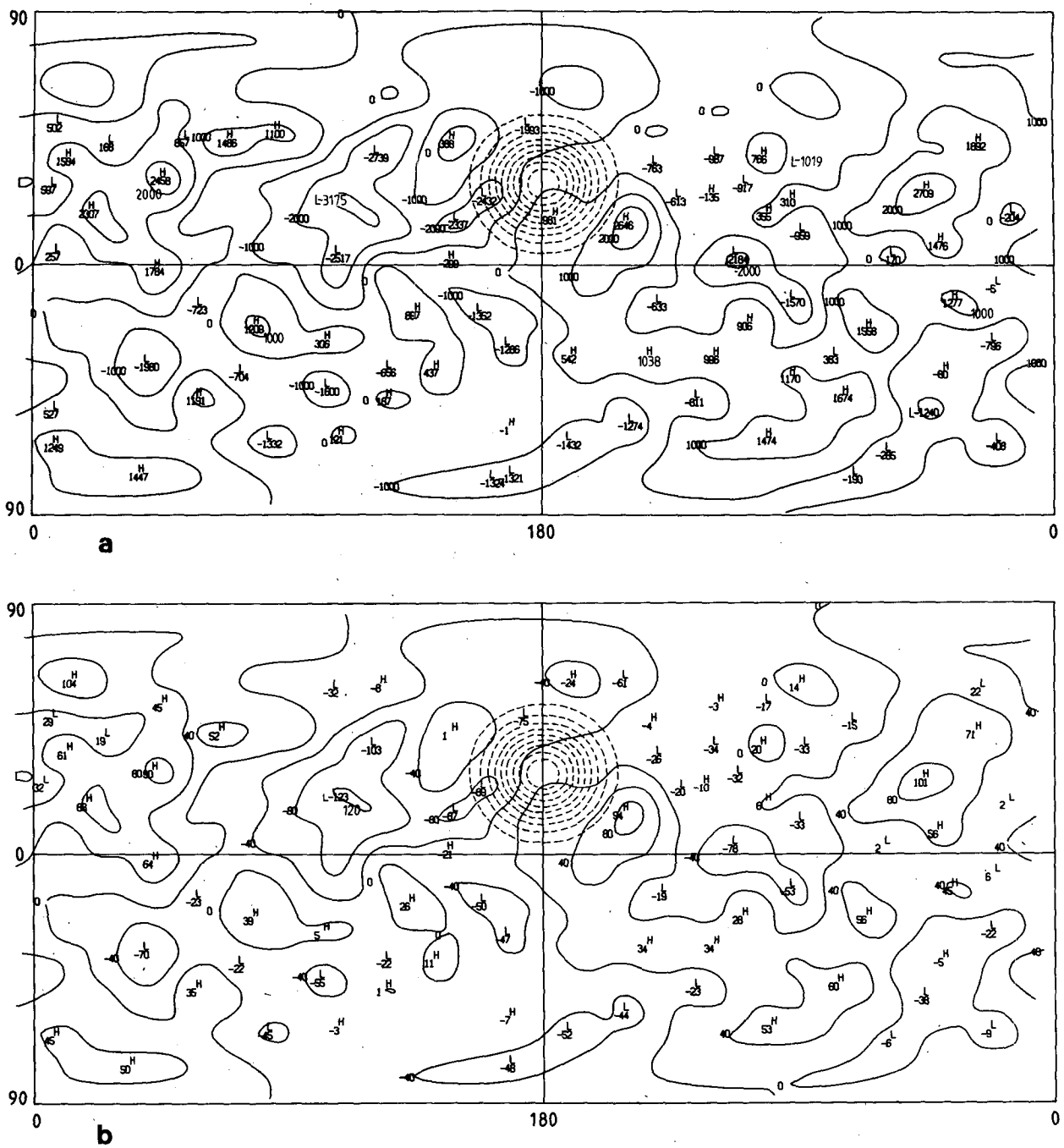

FIG. 4. Transient random phase equilibrium eddy ($m \neq 0$) streamfunctions in 10^4 m^2 s^{-1} for $|u_i|$ = 15.0 m s^{-1} and variable f, for (a) eastward initial flow and (b) westward initial flow. Also shown is the topography in meters (dashed line).

that there is a remarkable similarity between Fig. 7, and Fig. 5 which shows the nonlinear stationary equilibrium streamfunction. This similarity between linear and nonlinear solutions is quite different from the situation of initial eastward flow discussed above and in FS2 where the nonlinear and linear stationary flow fields differ drastically. It appears that for westward flow the linear steady state solution is a close approximation to the nonlinear equilibrium stationary streamfunction. That this is so for all three westward flows in Table 1 may be seen analytically by comparing α/β with $2(1 - \Gamma)/\Gamma$, as in Table 3. We see that in each case there is a very close correspondence between these two parameters and hence from Eqs. (2.5) and (2.15) between the stationary eddy streamfunctions.

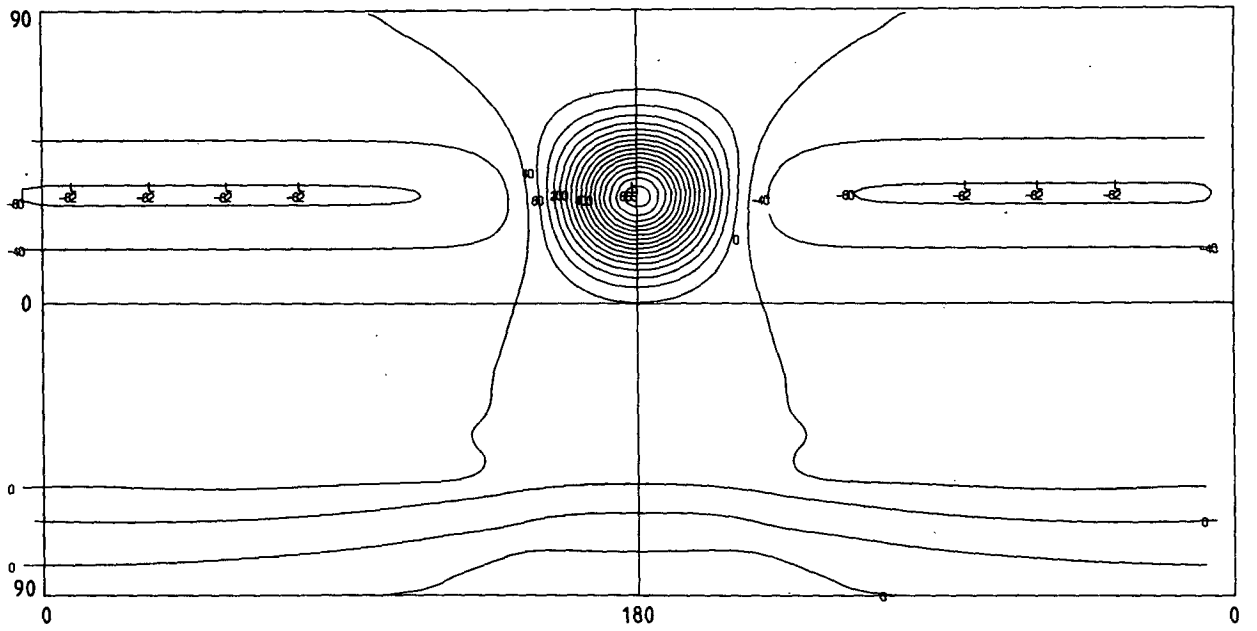

FIG. 5. Stationary equilibrium eddy streamfunction in 10^4 m^2 s^{-1} for westward initial flow with $u_i = -15.0$ m s^{-1} and with variable f.

c. *Discussion*

The similarity between the linear and nonlinear stationary solutions for westward initial flow and the drastic differences between linear and nonlinear stationary streamfunctions for initial eastward flow is perhaps puzzling. Since the nonlinear stationary solution for initial eastward flow is essentially a filtered version of the topography and is very similar qualitatively to both the linear and nonlinear streamfunctions for initial westward flow, what can be the significance of the linear steady state solution for initial eastward flow, which is so different from the other three? It is clear that if one integrates numerically the

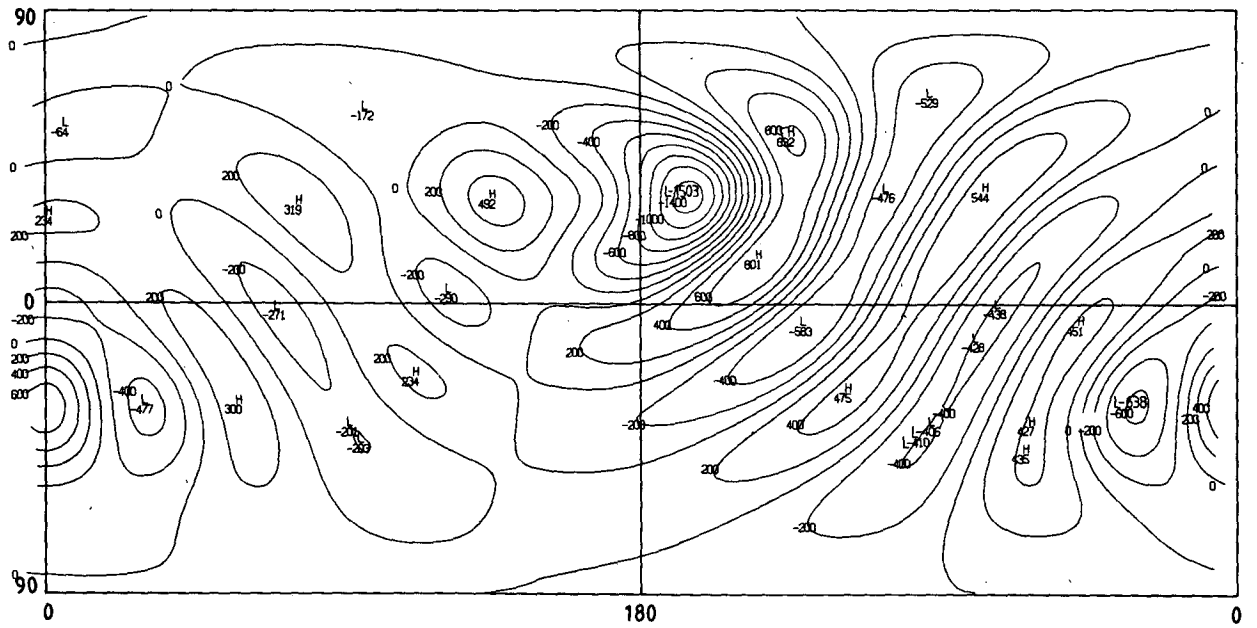

FIG. 6. Linear steady state eddy streamfunctions in 10^4 m^2 s^{-1} for eastward initial flow with $u_i = 15.0$ m s^{-1}, variable f and viscous dissipation.

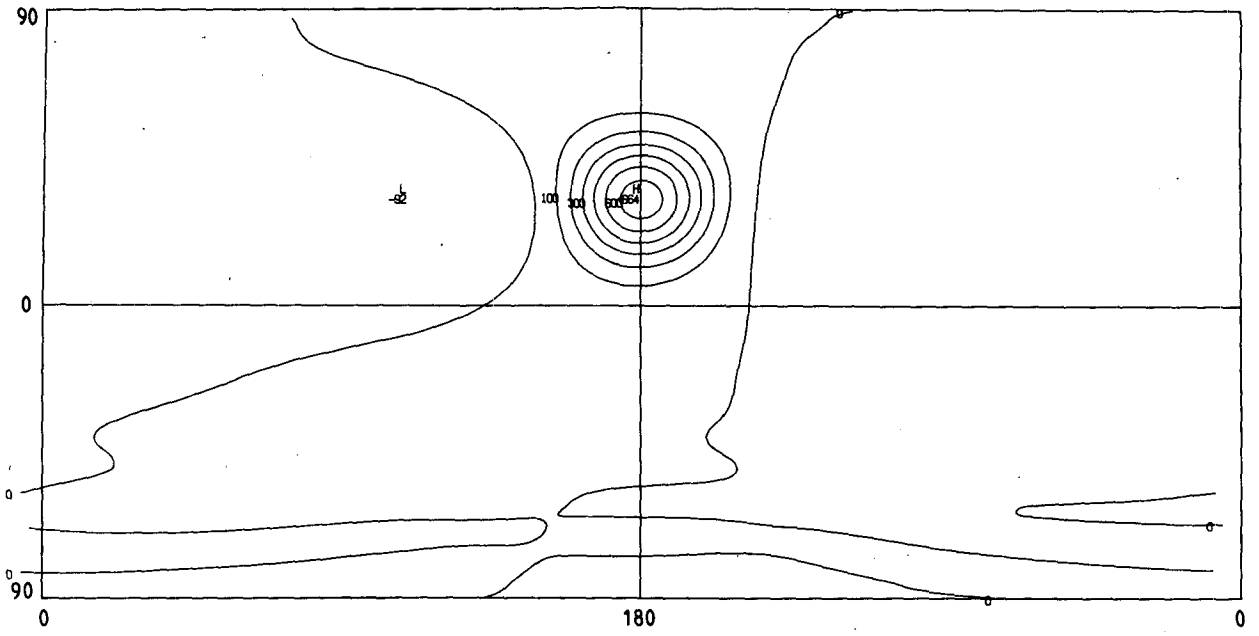

FIG. 7. Linear steady state eddy streamfunction in 10^4 m^2 s^{-1} for westward initial flow with $u_i = -15.0$ m s^{-1}, variable f and viscous dissipation.

inviscid nonlinear equation (2.1) with an eastward flow as the initial condition, the stationary solution is that corresponding to the statistical mechanical equilibrium solution rather than to the linear inviscid stationary solution (cf. also Edelmann, 1972). Similarly, it has also been found in planar geometry studies incorporating viscosity and using either the basic field equations or various closure assumptions (Bretherton and Haidvogel, 1976; Herring, 1977; Holloway, 1978) that there too the streamfunction expectation value is essentially a filtered version of the topographic field. In particular, it is found that the streamfunction is essentially positively correlated with the topography, with highs over mountains and lows over valleys. Thus the linear steady state solution in Fig. 6 where drag and diffusion are included cannot be a good approximation to the (quasi) stationary flow field for topographic turbulence either, at least for reasonable dissipation. This is because the transient eddy terms are not small.

Nevertheless, linear steady state solutions for initial eastward flows have been used with some success for understanding the results of short-term numerical simulations (Kasahara, 1966) and the atmospheric flow field (FS2 and references therein). It seemed surprising that Kasahara is able to explain the scale of the essentially transient disturbances in his studies using linear steady state solutions. However, it appears that the reason that linear steady state theory correctly predicts this scale in his relatively short-time integrations is because of the relation (2.13). That is, the linear transient waves are dominated by the same scales, determined largely by the quasi-resonant condition, as the linear stationary solutions. The transient wave field, of course, changes its structure with time due to the different phase speeds and damping of the different components as shown in Eq. (2.12). Thus we see that both the (short term) linear and (asymptotic) nonlinear equilibrium transient solutions conform with statement (2) of Section 3. However, because of the quasi-resonant nature of the linear solutions the change of the dominant scale with changing initial eastward flow is much more dramatic than for the nonlinear equilibrium transient solutions.

Linear steady state theory has also been useful for understanding the observed climatological stationary flow field in the upper troposphere in winter (FS2 and references therein). Perhaps this is due to the fact that the atmosphere behaves there more like a pulsating system with the zonal flow being periodically restored toward its initial value. It seems plausible that an ensemble average taken over short periods when the zonal flow is large may appear more like an ensemble of linear solutions. However, lower in the atmosphere (FS2), linear steady state theory is less successful in its predictions.

TABLE 3. Comparison of the ratio α/β with $2(1 - \Gamma)/\Gamma$ where $\Gamma = -\gamma > 0$ for westward flow with variable f and for different zonal winds u_i.

u_i (m s^{-1})	−27.5	−15.0	−7.8
α/β	3.189×10^1	6.002×10^1	1.174×10^2
$2(1 - \Gamma)/\Gamma$	3.175×10^1	5.974×10^1	1.167×10^2

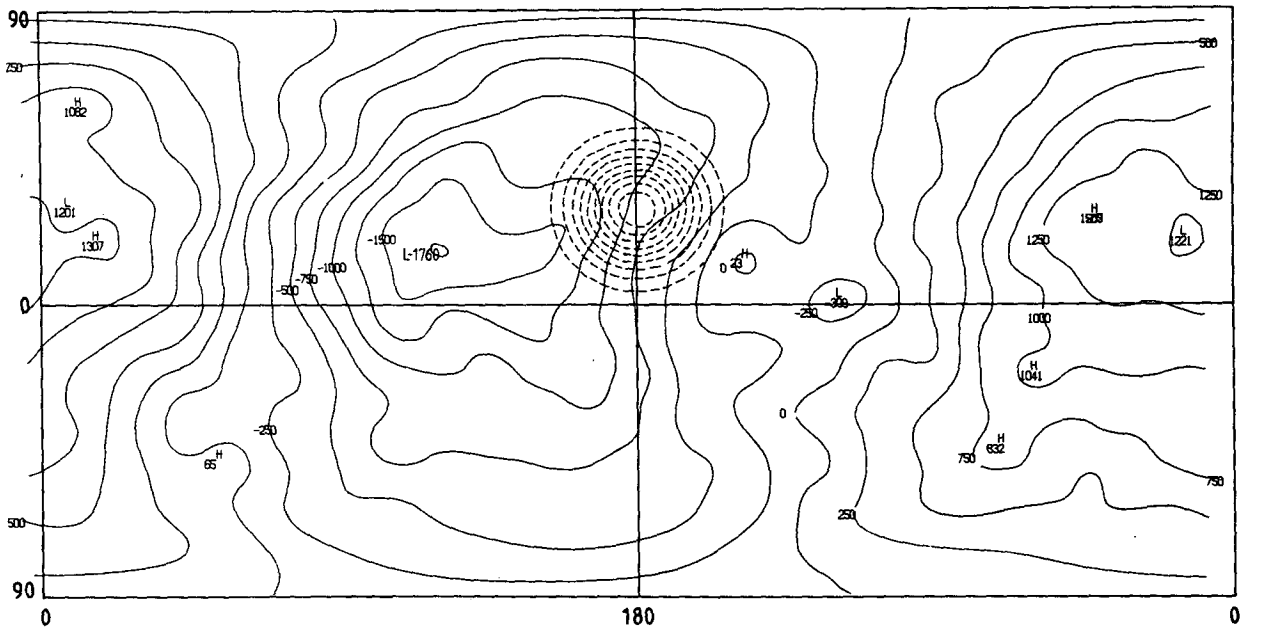

FIG. 8a. As in Fig. 4a, but for constant f.

5. Nonlinear and linear solutions with constant Coriolis parameter

Here we consider both the nonlinear equilibrium and linear streamfunctions for constant Coriolis parameter.

a. Nonlinear equilibrium solutions

Figs. 8a and b show the transient random phase eddy ($m \neq 0$) streamfunction and stationary eddy streamfunction for eastward initial flow with $u_i = 15.0$ m s^{-1} and with constant Coriolis parameter. Comparing Fig. 8a with Fig. 4a for the corresponding variable Coriolis parameter case, we see a considerable change in the dominant scale to $m = 1$ in Fig. 8a. Similarly the stationary eddy streamfunction is quite different from that in Fig. 5, in that it too has dominant zonal wavenumber $m = 1$.

For initial westward flow with $u_i = -15.0$ m s^{-1}, the eddy streamfunctions are very similar to those in

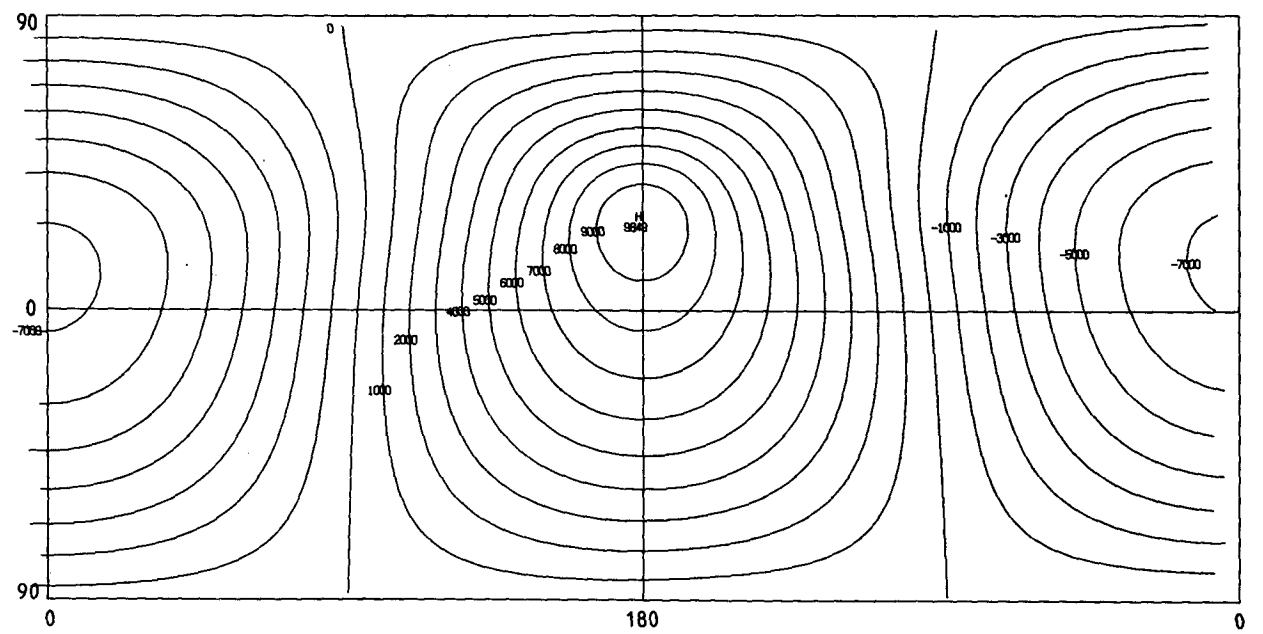

FIG. 8b. Stationary equilibrium streamfunction in 10^4 m^2 s^{-1} for eastward initial flow with $u_i = 15.0$ m s^{-1} and constant f.

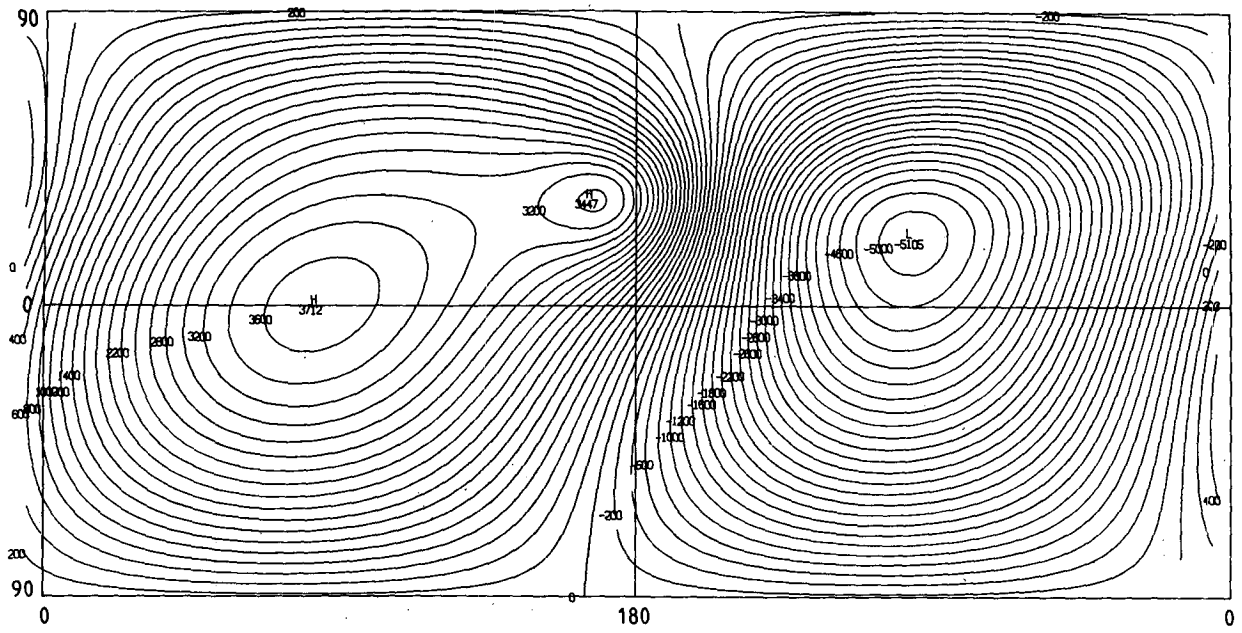

FIG. 9. As in Fig. 6, but for constant f.

Figs. 8a and b, but the transient eddy flow is slightly weaker (maximum strength -1357×10^4 m^2 s^{-1}) and the stationary eddy flow slightly stronger (maximum strength 9928×10^4 m^2 s^{-1}), as may also be seen from Figs. 1a and b.

For the other initial flows with $|u_i| = 27.5$ m s^{-1} (respectively $|u_i| = 7.8$ m s^{-1}) the eddy streamfunction fields are similar to those described above but with somewhat larger (respectively smaller) amplitudes.

b. Linear solutions

Fig. 9 shows the linear steady state eddy streamfunction for initial eastward flow with $u_i = 15.0$ m s^{-1}, constant f and with drag and diffusion as specified in Eq. (2.9). As discussed in Section 2, in the absence of drag and diffusion the resonant total wavenumber is exactly 1 and thus the linear steady state eddy streamfunction is infinite. In this sense, the finite eddy streamfunction in Fig. 9 is dominated by viscosity. Note that the asymmetry in Fig. 9 is caused by the drag and diffusion. Nevertheless it is interesting to note that both the linear steady state and stationary nonlinear eddy solutions have the largest $|m| = 1$ components; to this extent there is agreement between the solutions.

For initial westward flow with $u_i = -15.0$ m s^{-1}, the linear steady state solution is the mirror image of Fig. 9 reflected about 180° longitude. This might be expected on dynamical grounds and is easily seen mathematically from Section 2.

For both eastward and westward initial flows we note from Table 2 that as $|u_i|$ increases, α^0/β^0 approaches -2, and from Eq. (2.16) it is apparent that for $m > 1$ the inviscid linear steady state and the nonlinear stationary solutions approach each other. This is consistent with the expectation that linearization should be a better approximation for larger $|u_i|$. It is also consistent with the fact that for larger $|u_i|$ transients play a relatively less important role in the nonlinear solutions. However, for the nonlinear solutions the presence of even relatively small amounts of transients is sufficient to remove the singularity at $|m| = 1$ in Eq. (2.16), while for the linear solutions viscosity is needed. The fact that nonlinearity may act as an effective viscosity and thus removes sharp gradients has been discussed in some detail by Carnevale and Frederiksen (1982) (see also Leslie, 1973 and references therein).

c. Discussion

Again, from Eq. (2.13) we see that the linear transient waves are dominated by the same scales as the linear stationary solutions. Thus both linear and nonlinear transient eddy solutions are consistent with the qualitative behavior shown in Fig. 4 of Kasahara (1966). That is, the dominant zonal wavenumber is $|m| = 1$ for the case of constant Coriolis parameter, while smaller scales make more important contributions when the Coriolis parameter varies as in Fig. 5 of Kasahara. The stronger intensities of the transient eddies when the Coriolis parameter varies is consistent with the nonlinear equilibrium results but would not appear to be consistent with the linear results with the present drag and diffusion (cf. Figs. 6 and 9).

6. Conclusions

The spherical equivalent barotropic model has been used to study the transient and stationary eddies

produced when zonal solid body rotation currents flow eastward and westward over topography. Fully nonlinear statistical mechanical equilibrium solutions have been obtained and compared with linearized solutions and with the qualitative results of previous laboratory and numerical experiments. Cases involving both variable and constant Coriolis parameters (f) have been studied.

The statistical mechanical equilibrium solutions show that westward initial flow with variable f is stable in the sense that only very small amplitude transients are produced and the initial flow is practically unchanged. The stationary streamfunction then dominates the total flow field and there is excellent agreement between the linear steady state and nonlinear stationary solutions. Both also agree with the qualitative results of laboratory and numerical experiments.

The equilibrium solutions show that eastward initial flow with variable f is unstable; large amplitude transients are produced and the zonal flow direction changes to westward. The transient eddy streamfunction has much larger amplitude than the stationary contribution and dominates the total eddy flow field. The stationary equilibrium eddy streamfunction is essentially a filtered version of the topographic field and is very similar to that for initial westward flow but of reduced amplitude. In contrast, the linear steady state solutions are resonant or near resonant and differ dramatically from the nonlinear stationary solutions. It is shown that the reason linearized solutions may be useful in interpreting the results of short-time numerical experiments of eastward zonal flow over topography is that the linear transient waves are dominated by the same scales, determined largely by the quasi-resonance condition, as the linear stationary solutions. The application of linearized solutions for understanding the essentially eastward flow over topography in the atmosphere has also been discussed. The results of long-time numerical experiments, in particular the reversal of the zonal wind, are consistent with the nonlinear equilibrium solutions.

When the Coriolis parameter is taken to be constant, the nonlinear equilibrium solutions show that both initial eastward and westward flows produce considerably less transients than with initial eastward flow and variable f. Again the eastward flow reverses to westward while the westward flow remains that way although its strength is somewhat reduced. For both cases the transient and stationary eddy energy spectra are strongly peaked at zonal wavenumber $m = 1$ and the stationary streamfunction dominates the total eddy field. The corresponding linear steady state solutions have a resonance at total wavenumber $n = 1$ (i.e. at $|m| = 1, n = 1$) when the flow is inviscid, and large amplitude there when viscous dissipation is included. Both nonlinear and linear solutions have been compared with numerical experiments.

Acknowledgments. I am grateful to B. L. Sawford for discussing with me the linear transient solutions and for helpful comments on the manuscript. It is a pleasure to thank S. M. Kepert for his able assistance in this study. I wish to thank J. Evans for typing the manuscript.

REFERENCES

Bretherton, F. P., and D. B. Haidvogel, 1976: Two-dimensional turbulence above topography. *J. Fluid Mech.*, **78**, 129–154.

Carnevale, G. F., 1979: Statistical dynamics of nonequilibrium fluid systems. Ph.D thesis, Harvard University, 169 pp.

——, U. Frish and R. Salmon, 1981: H-Theorems in fluid dynamics. *J. Phys. A*, **14**, 1701–1718.

——, and J. S. Frederiksen, 1982: A statistical dynamical theory of strongly nonlinear interval gravity waves. Submitted to *Geophys. Astrophys. Fluid Dyn.*

Edelmann, W., 1972: Numerical experiments with a barotropic current across mountains. *Beitr. Phys. Atmos.*, **45**, 196–229.

Egger, J., 1970: On the simulation of subgrid orographic effects in numerical forecasting. *J. Atmos. Sci.*, **27**, 896–902.

——, and W. Metz, 1981: On the mountain torque in barotropic planetary flow. *Quart. J. Roy. Meteor. Soc.*, **107**, 299–312.

Frederiksen, J. S., and B. L. Sawford, 1980: Statistical dynamics of two-dimensional inviscid flow on a sphere. *J. Atmos. Sci.*, **37**, 717–732.

——, and ——, 1981: Topographic waves in nonlinear and linear spherical barotropic models. *J. Atmos. Sci.*, **38**, 69–86.

Frenzen, P., 1955: Westerly flow past an obstacle in a rotating hemispherical shell. *Bull. Amer. Meteor. Soc.*, **36**, 204–210.

Fultz, D., and R. R. Long, 1951: Two-dimensional flow around a circular barrier in a rotating spherical shell. *Tellus*, **3**, 61–68.

——, and P. Frenzen, 1955: A note on certain interesting ageostrophic motions in a rotating hemispherical shell. *J. Meteor.*, **12**, 323–338.

Herring, J. R., 1977: Two-dimensional topographic turbulence. *J. Atmos. Sci.*, **34**, 1731–1750.

Holloway, G., 1978: A spectral theory of nonlinear barotropic motion above irregular topography. *J. Phys. Oceanogr.*, **8**, 414–427.

Holton, J. R., 1979: *An Introduction to Dynamic Meteorology*, 2nd ed. Academic Press, 391 pp.

Kasahara, A., 1966: The dynamical influence of orography on the large scale motion of the atmosphere. *J. Atmos. Sci.*, **23**, 259–270.

Kraichnan, R. H., 1959: The structure of isotropic turbulence at very high Reynolds numbers. *J. Fluid Mech.*, **5**, 497–543.

Leith, C. E., 1971: Atmospheric predictability and two-dimensional turbulence. *J. Atmos. Sci.*, **28**, 145–161.

Leslie, D. C., 1973: *Developments in the Theory of Turbulence.* Clarendon Press, 368 pp.

Long, R. R., 1952: The flow of a liquid past a barrier in a rotating spherical shell. *J. Meteor.*, **9**, 187–199.

Salmon, R., G. Holloway and M. C. Hendershott, 1976: The equilibrium statistical mechanics of simple quasi-geostrophic models. *J. Fluid Mech.*, **76**, 691–703.

Sawford, B. L., and J. S. Frederiksen, 1982: Mountain torque and angular momentum in barotropic planetary flows: Equilibrium solutions. Submitted to *Quart. J. Roy. Meteor. Soc.*

Thompson, P. D., 1974: The integral invariants of two-dimensional inviscid flow and their role in the theory of two-dimensional turbulence. *J. Atmos. Sci.*, **31**, 1453–1457.

Vergeiner, I., and Y. Ogura, 1972: A numerical shallow-fluid model including orography with a variable grid. *J. Atmos. Sci.*, **29**, 270–284.